JACS Au
AN OPEN ACCESS JOURNAL OF THE AMERICAN CHEMICAL SOCIETY

Counterion Effects in $[Ru(bpy)_3](X)_2$-Photocatalyzed Energy Transfer Reactions

Juliette Zanzi, Zachary Pastorel, Carine Duhayon, Elise Lognon, Christophe Coudret, Antonio Monari, Isabelle M. Dixon,* Yves Canac,* Michael Smietana,* and Olivier Baslé*

Cite This: *JACS Au* 2024, 4, 3049−3057

ABSTRACT: Photocatalysis that uses the energy of light to promote chemical transformations by exploiting the reactivity of excited-state molecules is at the heart of a virtuous dynamic within the chemical community. Visible-light metal-based photosensitizers are most prominent in organic synthesis, thanks to their versatile ligand structure tunability allowing to adjust photocatalytic properties toward specific applications. Nevertheless, a large majority of these photocatalysts are cationic species whose counterion effects remain underestimated and overlooked. In this report, we show that modification of the X counterions constitutive of $[Ru(bpy)_3](X)_2$ photocatalysts modulates their catalytic activities in intermolecular [2 + 2] cycloaddition reactions operating through triplet−triplet energy transfer (TTEnT). Particularly noteworthy is the dramatic impact observed in low-dielectric constant solvent over the excited-state quenching coefficient, which varies by two orders of magnitude depending on whether X is a large weakly bound ($BAr^F{}_4{}^-$) or a tightly bound (TsO^-) anion. In addition, the counterion identity also greatly affects the photophysical properties of the cationic ruthenium complex, with $[Ru(bpy)_3](BAr^F{}_4)_2$ exhibiting the shortest ^{3}MLCT excited-state lifetime, highest excited state energy, and highest photostability, enabling remarkably enhanced performance (up to >1000 TON at a low 500 ppm catalyst loading) in TTEnT photocatalysis. These findings supported by density functional theory-based calculations demonstrate that counterions have a critical role in modulating cationic transition metal-based photocatalyst potency, a parameter that should be taken into consideration also when developing energy transfer-triggered processes.

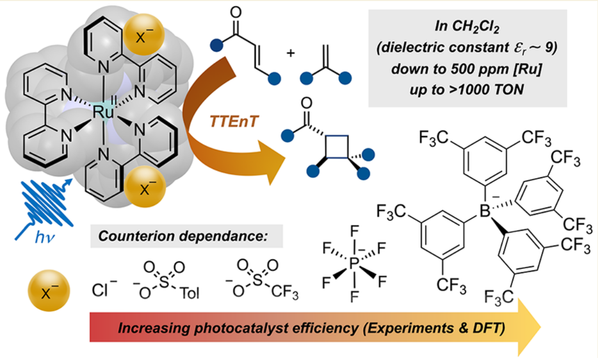

KEYWORDS: *counterion effects, triplet energy transfer, photocatalysis, [2 + 2] cycloaddition, ruthenium complex, DFT*

INTRODUCTION

Photocatalysis under visible-light irradiation has witnessed tremendous successes in recent years in a wide variety of applications[1−7] and has notably initiated a paradigm shift in organic synthesis.[8−19] Within the design of efficient molecular photocatalytic systems, the architecture of metal-based photocatalysts can easily be tuned to efficiently achieve the desired photochemical properties required to promote specific transformations.[20] Thanks to their strong absorption in the visible region, rapid intersystem crossing, and long-lived triplet excited state, polypyridyl ruthenium(II) and cyclometalated iridium(III) complexes are the most widely explored classes of photoredox catalysts and photosensitizers.[21] The common method to manipulate excited-state properties of such photocatalysts relies on modifying the ligand scaffold around the metal center: a *modus operandi* that has provided access to a plethora of photocatalysts covering a broad range of redox potentials and triplet excited state energies.[22,23] Importantly, a large majority of these Ir(III) and Ru(II) complexes, but also of emerging earth-abundant transition metal-based luminescent complexes,[24−31] are cationic species associated with counterion(s) to ensure charge balance of the molecular photocatalysts. Nevertheless, while photocatalytic reaction cycles are usually modeled considering the properties of the sole organometallic cation, the true nature of the photocatalyst is that of a salt in which the anions could play a role beyond the one of mere spectators.[32−38] In this respect, recent reports have brought to light the influence of counterion identity on the efficiency of single electron transfer (SET) processes operated by cationic iridium and ruthenium photoredox catalysts (Figure 1A).[39−42] However, despite the fact that both SET and energy transfer (EnT) photocatalyses rely on the triplet metal-to-ligand charge-transfer (^{3}MLCT) excited state of the photocatalyst, counterion effects on EnT processes have not been demonstrated yet. In triplet−triplet energy

Received: April 30, 2024
Revised: July 15, 2024
Accepted: July 15, 2024
Published: July 24, 2024

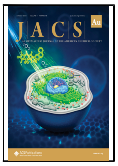

https://doi.org/10.1021/jacsau.4c00384

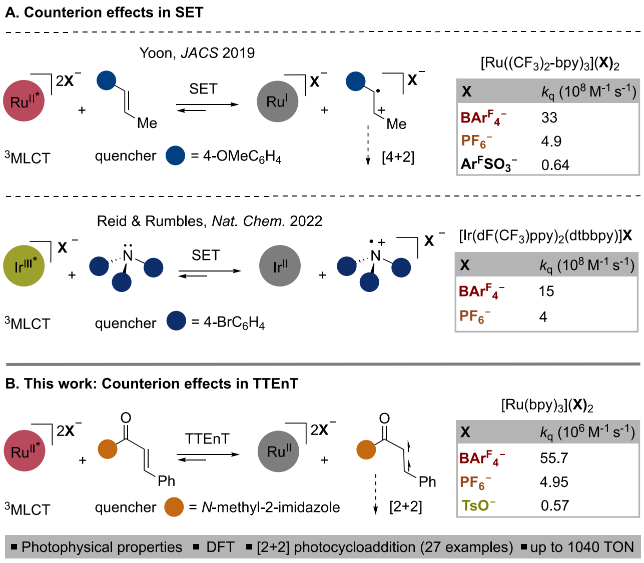

Figure 1. Counterion dependence in photochemical processes. (A) Previously reported counterion effects on single electron transfer (SET). (B) Counterion effects in $[Ru(bpy)_3](X)_2$-catalyzed intermolecular [2 + 2] cycloaddition enabled by energy transfer. Bimolecular quenching rate constant (k_q). 3,5-Bis(trifluoromethyl)benzenesulfonate ($Ar^FSO_3^-$). Turnover number (TON).

transfer (TTEnT) processes, a burgeoning field of research with a wide range of synthetic applications,[43−46] the photocatalyst is excited by the direct absorption of visible light and subsequently transfers its triplet excited state energy to a desired substrate, opening otherwise elusive relaxation channels and photoreactive routes, leading to original chemical transformations.[47] Herein, we show that modification of the X counterions in the emblematic $[Ru(bpy)_3](X)_2$ complex series has a dramatic impact on their photophysical properties and photocatalytic activity in TTEnT. Specifically, we demonstrate that large noncoordinating tetrakis[3,5-bis(trifluoromethyl)phenyl]borate ($BAr^F_4{}^-$) anions are highly beneficial, giving rise to much higher photocatalytic activity (up to >1000 TON) in intermolecular [2 + 2] cycloaddition reactions of olefins to yield cyclobutanes (Figure 1B).[48] We rationalize the superior photocatalytic performance of $[Ru(bpy)_3](BAr^F_4)_2$ over its congeners on the basis of experimental and density functional theory (DFT) studies that indicate a favorable increase in the energy of both the ^{3}MLCT and the metal-centered (^{3}MC) excited states, which are respectively responsible for a larger energy transfer driving force and an improved photostability. Our results provide fundamental insights into how counterions impact cationic transition metal-based photocatalyst potency in triplet energy transfer-activated reactions, a topic of great interest but surprisingly overlooked so far in the literature.

RESULTS AND DISCUSSION

As a model reaction to evaluate the impact of counterion effect in TTEnT photocatalysis, we selected the [2 + 2]-cycloaddition of α,β-unsaturated 2-acyl imidazole **1a** with styrene **2a** using $[Ru(bpy)_3](X)_2$ as a triplet sensitizer under visible-light irradiation. The choice of the reaction has been made in light of recent studies on "triplet activation" of **1a**,[49−52] in particular that of Yoon and co-workers,[50] who showed that the presence of trifluoromethanesulfonic acid as a Brønsted acid cocatalyst is strictly necessary to efficiently promote this $[Ru(bpy)_3]^{2+}$-catalyzed [2 + 2] photocycloaddition in acetonitrile. The effect was justified by the fact that the protonated acyl imidazole substrate is a better energy acceptor for the triplet excited state of $[Ru(bpy)_3](Cl)_2$*. We therefore assumed that by modifying the counterions of $[Ru(bpy)_3](X)_2$ photosensitizers and assessing their ability to promote the aforementioned [2 + 2] photocycloaddition in the absence of any additive, we could acquire the first evidence of counterion effects in TTEnT photocatalysis. The results of the initial screening of a series of Ru(II) photosensitizers for the intermolecular [2 + 2] cycloaddition between **1a** and **2a** are summarized in Table 1.

Table 1. Initial Screening of Counterion Effects on EnT[a]

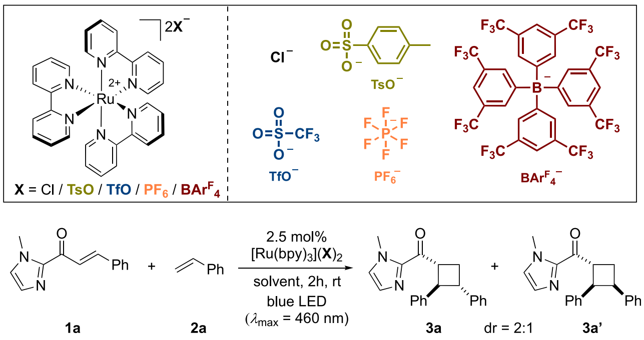

X⁻ =	Cl⁻	TsO⁻	TfO⁻	PF$_6$⁻	BAr$^F_4$⁻
yield[a] (in CH$_3$CN)	5	31	30	30	29
yield[b] (in CH$_2$Cl$_2$)	nd[c]	8	22	26	43

[a]Reaction conditions: **1a** (0.1 mmol), **2a** (1 mmol), $[Ru(bpy)_3](X)_2$ (2.5.10^{-3} mmol), degassed solvent (2 mL), and blue LED irradiation (λ_{max} = 460 nm) for 2 h under Ar. [b]Yield in % of **3a+3a′** determined by ^{1}H NMR using 1,3,5-trimethoxybenzene as an internal standard. [c]Products **3** were not detected by ^{1}H NMR.

Under the standard conditions, using 2.5 mol % of $[Ru(bpy)_3](X)_2$ as a sensitizer under blue-light irradiation, the rates of the photocycloaddition performed in either acetonitrile or dichloromethane as solvent were compared after 2 h of reaction. $[Ru(bpy)_3](Cl)_2$ proved incompetent as a photosensitizer to promote the desired transformation, affording a very low 5% yield of the cyclobutane products in acetonitrile and displaying a complete lack of catalytic activity in dichloromethane, and was therefore left out for the rest of the experimental study.[50,53,54] On the other hand, using *p*-toluenesulfonate (TsO⁻), trifluoromethanesulfonate (TfO⁻), hexafluorophosphate (PF_6^-), or $BAr^F_4{}^-$ anions proved beneficial, and similar yields (~30%) of the desired cyclobutane products were obtained in acetonitrile after 2 h. More interestingly, a striking difference in reaction rates was observed in dichloromethane depending on the counterion identity. While up to 43% yield of the [2 + 2]-cycloaddition products was obtained after 2 h of irradiation using the $[Ru(bpy)_3](BAr^F_4)_2$ photocatalyst, the reaction proceeded to 26% yield with $[Ru(bpy)_3](PF_6)_2$, 22% with $[Ru(bpy)_3](TfO)_2$, and only 8% yield with $[Ru(bpy)_3](TsO)_2$.

In order to gain a better understanding of the parameters influencing the catalytic performances of this series of $[Ru(bpy)_3](X)_2$ photosensitizers, their optical properties were recorded in both acetonitrile and dichloromethane solutions. In acetonitrile, characterized by relatively high dielectric constant (ε_r ~ 37) impeding ion association, the properties of the ground state and $[Ru(bpy)_3]^{2+*}$ excited state

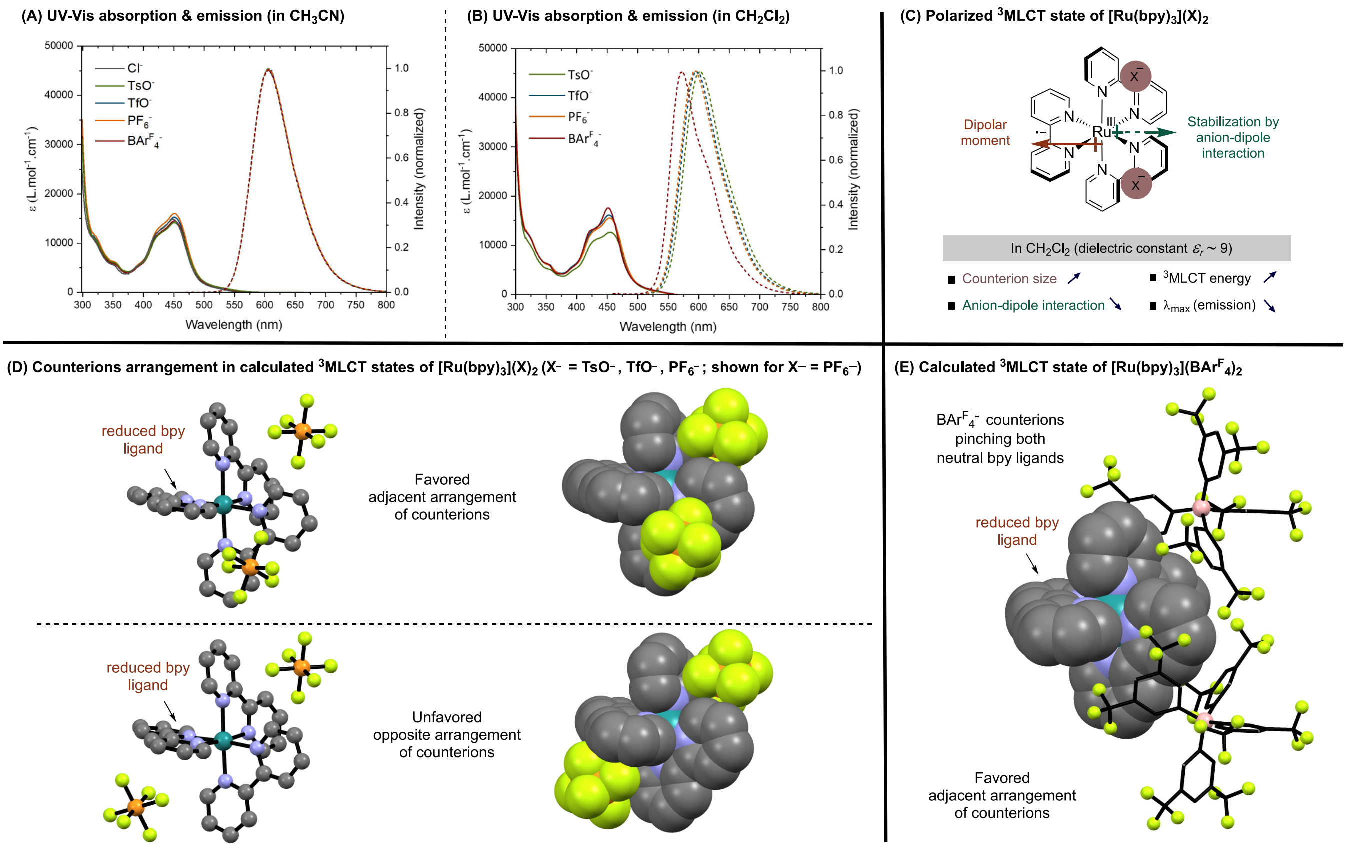

Figure 2. Counterion effect on absorption (solid lines) and emission (dashed lines, λ_{ex} = 450 nm) properties of $[Ru(bpy)_3](X)_2$ in acetonitrile (A) and in dichloromethane (B) at 25 °C. (C) ^{3}MLCT state of $[Ru(bpy)_3](X)_2$. (D) Opposite and adjacent arrangements of counterions in calculated ^{3}MLCT states of $[Ru(bpy)_3](X)_2$ shown for $X^- = PF_6^-$ in ball and stick (left) and space-filling (right) models (and Figure S22 for $X^- = Cl^-$). (E) Specific arrangement of counterions in the calculated ^{3}MLCT state of $[Ru(bpy)_3](BAr^F{}_4)_2$.

of solvated $[Ru(bpy)_3](X)_2$ salts should not be significantly affected by the nature of the counterion. Indeed, all complexes exhibited a similar metal-to-ligand charge-transfer (MLCT) absorption band at λ_{max} = 451 nm with similar molar extinction coefficients (15,000 M^{-1} cm^{-1}) and demonstrated superimposable emission spectra with λ_{em} = 605 nm (Figure 2A). In dichloromethane ($\varepsilon_r \sim 9$), on the other hand, while the impact of counterion identity on absorption spectra was modest with only a slight increase of molar extinction coefficients from the more coordinating TsO^- anion to the least coordinating $BAr^F{}_4{}^-$,[55] differences were more significant in emission spectroscopy (Figure 2B).[56] First, the emission of the TsO^- complex is characterized by a maximum at 604 nm/2.053 eV, and then the TfO^- and PF_6^- complexes showed a slight hypsochromic shift (λ_{em} = 598 nm/2.073 eV and 596 nm/2.080 eV, respectively) and finally the complex with the largest and least coordinating $BAr^F{}_4{}^-$ ions exhibited the most blue-shifted emission at λ_{em} = 575 nm/2.156 eV, up by 29 nm/0.103 eV. This relative ordering was satisfactorily reproduced by DFT ΔSCF calculations (Table S24). In dichloromethane of low dielectric constant, the emission energy of ion pairs thus seems to correlate with the charge density of the counterions. In fact, in the MLCT state, the transferred electron is localized on a single bipyridine ligand inducing a dipole moment in the $[(bpy^{\bullet -})Ru^{III}(bpy)_2]^{2+*}$ excited state of C_2 symmetry,[57−59] which can be stabilized by anion−dipole interaction with the paired anions positioned away from the formally reduced ligand (Figure 2C). The extent of this stabilization is inversely correlated with the counterion size.[60] The blue-shifted emission of $[Ru(bpy)_3](BAr^F{}_4)_2$ reflects its increased ^{3}MLCT energy, which is 0.103 eV/2.4 kcal/mol higher than the triplet energy of $[Ru(bpy)_3](TsO)_2$, which could in part account for the improved performance of the $BAr^F{}_4{}^-$ photocatalyst by increasing the driving force for energy transfer from its triplet state (E_T = 49.7 kcal/mol)[61] to the acyl imidazole substrate **1a** (E_T = 47.6 kcal/mol).[50] The GS-^{3}MLCT gaps for $[Ru(bpy)_3](X)_2$ complexes have been computed as the difference in their electronic energies at their respective equilibrium geometries in dichloromethane, as reported in Table S23. They follow a trend that perfectly reflects the experimental observations: the gap goes from 46.6 kcal/mol for $[Ru(bpy)_3](BAr^F{}_4)_2$ to 45.4 kcal/mol for $[Ru(bpy)_3](PF_6)_2$, 44.4 kcal/mol for $[Ru(bpy)_3](TfO)_2$ and 44.1 kcal/mol for $[Ru(bpy)_3](TsO)_2$. These values correspond to the electrostatically favorable adjacent arrangement of the counterions, i.e., counterions in neighboring quadrants and remote from the formally reduced bpy ligand, as opposed to an unfavorable opposite arrangement where counterions would be diametrically opposed with respect to the metal center and with one counterion in the immediate vicinity of the reduced bpy ligand ($\Delta E_{adj/opp}$ = 0.6−3.7 kcal/mol) (Figure 2D and Table S23). Noteworthy is the ^{3}MLCT state of $[Ru(bpy)_3](BAr^F{}_4)_2$ with an adjacent arrangement of the counterions that is slightly different from the others. Due to their bulkiness and specific geometry, the $BAr^F{}_4{}^-$ counterions are pinching both neutral bpy ligands in a clip-like configuration (Figure 2E, Figure S23 and the SI for related discussions and additional visual representations).

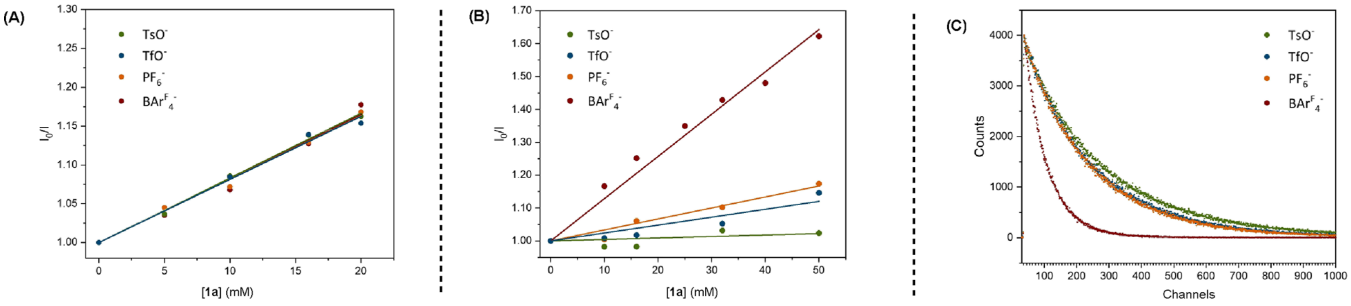

Figure 3. Stern−Volmer plots for excited-state quenching of $[Ru(bpy)_3]X)_2$ by **1a** in acetonitrile (A) and in dichloromethane (B). Excited-state lifetime of $[Ru(bpy)_3](X)_2$ in deaerated CH_2Cl_2 (C).

Table 2. Counterion Dependence of the Optical Properties and Quenching Constants of $[Ru(bpy)_3](X)_2$ in Dichloromethane[a]

X^-	ε ($M^{-1}\cdot cm^{-1}$)	λ_{em} (nm)	K_{sv} (M^{-1})	τ_0 (ns)[b]	k_q (10^6 M^{-1} s^{-1})[c]	k_r (10^4 s^{-1})[d]	k_{nr} (10^6 s^{-1})[e]	Φ_{lum}
TsO^-	12,450	604	0.46	804	0.57	8.71	1.16	0.070
TfO^-	15,340	598	2.40	694	3.46	7.92	1.36	0.055
PF_6^-	16,020	596	3.34	675	4.95	7.41	1.41	0.050
$BArF^-$	17,530	575	12.86	231	55.67	9.96	4.23	0.023

[a] Photophysical data were obtained in dry, deaerated CH_2Cl_2 at 293 K. ε is the molar extinction coefficient at the lowest-energy absorption band maximum, and λ_{em} is the wavelength of the emission band maximum. [b] λ_{exc} = 455 nm. [c] $k_q = K_{sv}/\tau_0$. [d] $k_r = \Phi_{lum}/\tau_0$. [e] $k_{nr} = (1 - \Phi_{lum})/\tau_0$.

To gain further insight into the influence of counterion on energy transfer performance, we conducted Stern−Volmer experiments of intermolecular deactivation of the triplet excited states of ruthenium complexes by an increasing concentration of substrate **1a** as a quencher.[62] First, in agreement with the very similar catalytic activities observed in acetonitrile (*vide supra*, Table 1), all excited complexes demonstrated the same ability to be quenched by **1a** with a Stern−Volmer rate constant (K_{sv}) of ~8.2 M^{-1} (Figure 3A). In sharp contrast, Stern−Volmer plots measured in dichloromethane evidenced large differences depending on the identity of the counterions (Figure 3B). The quenching rate constant of the photoexcited catalysts by the substrate increased by a factor of 25 from the TsO^- to the $BAr^F_4{}^-$ counterion, also in line with the markedly superior photocatalytic performance of the latter. Then, their ^{3}MLCT excited-state lifetimes (τ_o) were measured in dichloromethane and once again a significant influence of the counterions was established. The $BAr^F_4{}^-$ complex evidenced the shortest excited-state lifetime (τ_o = 231 ns), which is almost four times shorter than that of the TsO^- complex (τ_o = 804 ns). This behavior is usually rationalized by a reduced energy gap between the ^{3}MLCT excited state and the low-lying metal-centered (^{3}MC) excited states of $[Ru(bpy)_3]^{2+}$, which facilitates the ^{3}MLCT-^{3}MC internal conversion enabling more efficient nonradiative deactivation pathways,[63,64] as reflected in the decreased luminescence quantum yield (Φ_{lum}, Table 2). The better performance of the $[Ru(bpy)_3](BAr^F_4)_2$ photocatalyst is all the more remarkable that its excited state lifetime is significantly reduced, which decreases the probability of encountering the substrate for productive energy transfer. The actual quenching rate constant (k_q) for this series of $[Ru(bpy)_3](X)_2$ photosensitizers could be accessed thanks to the Stern−Volmer relationship ($K_{sv} = k_q\ \tau_o$), and remarkably, a decrease by two orders of magnitude between the large and noncoordinating $BAr^F_4{}^-$ and the small coordinating TsO^- was determined, highlighting the impressive superiority of $[Ru(bpy)_3](BAr^F_4)_2$ to efficiently transfer its triplet energy to the α,β-unsaturated 2-acyl imidazole substrate **1a**. This reactivity could be explained by the higher tendency of the bulky $BAr^F_4{}^-$ counterions to dissociate from their cation to form solvent-separated ion pairs,[40,65] thus unshielding the $[Ru(bpy)_3]^{2+}$ cation in its triplet excited state and facilitating collisions with the substrate for effective triplet−triplet energy transfer.[66,67]

Another parameter that plays an important role in photocatalysis is the photostability of catalysts.[63] Nevertheless, $[Ru(bpy)_3]^{2+}$ complexes are recognized for their relatively low photostability in nonpolar solvents such as dichloromethane. In fact, photodecomposition of $[Ru(bpy)_3]^{2+}$ is known to operate through photodissociation of a bipyridine (bpy) ligand, a phenomenon that becomes significant in solvent of low dielectric constant with strongly coordinating anions that can substitute the bpy ligand leading to photocatalytically inactive $Ru(bpy)_2X_2$ complexes such as $Ru(bpy)_2Cl_2$.[53,54] Therefore, the photostability of our series of $[Ru(bpy)_3](X)_2$ complexes was investigated by monitoring the luminescence intensity of CH_2Cl_2 solutions irradiated with blue LEDs (λ_{max} = 460 nm). The decrease of luminescence intensity (I/I_0) as a function of irradiation time is presented in Figure 4. As expected, $[Ru(bpy)_3](TsO)_2$ with the most coordinating counterion in the series evidenced the lowest photostability, leading to almost complete decomposition (>85%) after only

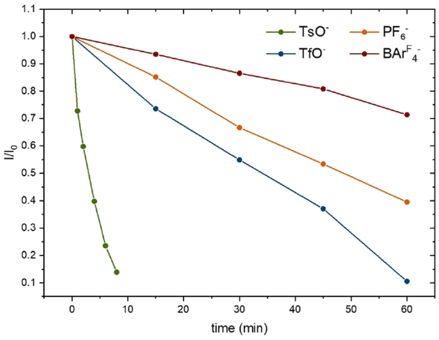

Figure 4. Photostability of $[Ru(bpy)_3](X)_2$ complexes in dichloromethane (8 mM) at 25 °C under 50W blue LED (λ_{max} = 460 nm) irradiation.

10 min of irradiation. A significantly lower decomposition rate was measured for $[Ru(bpy)_3](TfO)_2$ and $[Ru(bpy)_3](PF_6)_2$, which maintained 25 and 40% of their initial luminescence after 1 h of irradiation, respectively. Interestingly, $[Ru(bpy)_3](BAr^F{}_4)_2$ exhibited the highest photostability being roughly twice as robust as $[Ru(bpy)_3](PF_6)_2$. The superior photostability of $[Ru(bpy)_3](BAr^F{}_4)_2$ compared to $[Ru(bpy)_3](PF_6)_2$, both involving noncoordinating ions, is of note given its increased ^{3}MLCT state energy. DFT calculations were performed to optimize the lowest MLCT and MC states for the PF_6^- and $BAr^F{}_4^-$ complexes (and the bare cation as a reference, SI, since all our previous calculations on $[Ru(bpy)_3]^{2+}$ were conducted using MeCN as implicit solvent).[68−71] Indeed, several types of MC states may be invoked, whose electronic structures differ in the nature of the populated $d_{\sigma*}$ orbital. As a global picture, when populating a d_{z^2}-like orbital, two major Ru−N elongations will occur involving two pyridines from *separate* ligands in tris(bidentate) complexes such as $Ru(bpy)_3^{2+}$, leading to what we termed MC_{trans} states. On the contrary, if a $d_{x^2-y^2}$-like orbital is populated, three or four major elongations will occur, two of which involving *the same* ligand, leading to MC_{cis} states. For this reason, photoinstability issues due to ligand loss have been suggested to involve preferably $d_{x^2-y^2}$-based MC_{cis} states while nonradiative deactivation has been suggested to proceed preferably through d_{z^2}-based MC_{trans} states (Figure 5).[68,70,71]

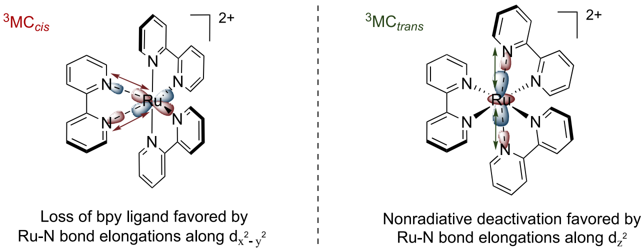

Figure 5. Schematic representation of ^{3}MC states of $[Ru(bpy)_3]^{2+}$ with elongation along either $d_{x^2-y^2}$ ($^3MC_{cis}$, left) or d_{z^2} ($^3MC_{trans}$, right).

The calculated Jablonski diagram (Figure 6) shows that MC_{cis} states (red dots) are higher in energy and better separated from MC_{trans} states (green dashes) for the $BAr^F{}_4^-$ complex compared to the PF_6^- analogue, in line with the higher photostability of the former. Besides, since the ^{3}MLCT lifetime is long enough to allow relaxation of the anions,[40] the globally lowest state, labeled as ^{3}MLCT-adj and presenting adjacent anions, is the one that should be considered as the most populated. The gap between ^{3}MLCT-adj and $^3MC_{trans}$-adj is smaller for $[Ru(bpy)_3](BAr^F{}_4)_2$ (5.3 kcal/mol) than for $[Ru(bpy)_3](PF_6)_2$ (7.0 kcal/mol), in agreement with the shorter MLCT lifetime of the $BAr^F{}_4^-$ complex (*vide supra* Figure 3C and Table 2).

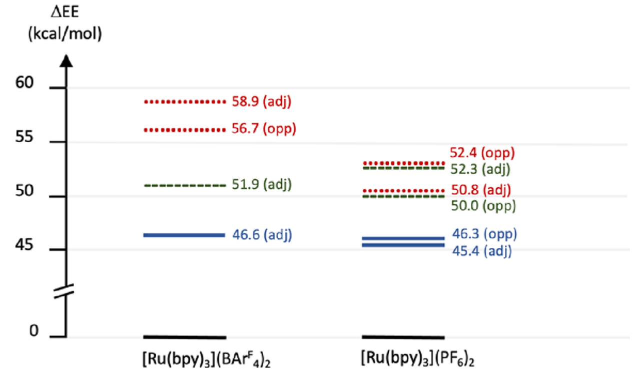

Figure 6. Diagram schematizing the relative electronic energies of optimized GS (black), ^{3}MLCT (blue lines), $^3MC_{cis}$ (red dots), and $^3MC_{trans}$ (green dashes) states for $[Ru(bpy)_3](BAr^F{}_4)_2$ and $[Ru(bpy)_3](PF_6)_2$ complexes. Multiple states of the same color indicate various anion arrangements, such as adjacent (adj) and opposite (opp) (see text, Tables S22, S23, S25 and the SI).

After demonstrating the high photostability of the $BAr^F{}_4^-$ catalyst and its excellent ability to transfer its triplet energy to substrate **1a** in dichloromethane, we optimized the conditions for the [2 + 2] photocycloaddition reaction in the presence of styrene **2a** as a partner. First, using 2.5 mol % of $[Ru(bpy)_3](BAr^F{}_4)_2$ as photocatalyst and by increasing the reaction concentration from 0.05 to 0.1 M, the rate of the cycloaddition after 2 h of irradiation under blue LEDs (λ_{max} = 460 nm) improved to reach 56% yield of the desired product (Table 3, entries 1 and 2). Interestingly, a decrease of the photocatalyst loading from 2.5 to 1 mol % (Table 3, entry 3) and 0.5 mol % (Table 3, entry 4) did not significantly affect the productivity since very similar results were obtained after 2 h of reaction, allowing to reach a TON above 100 in the latter case. The optimized conditions used a low photocatalyst loading of 0.5 mol % and a reaction concentration of 0.2 M (Table 3, entry 5), which allowed full conversion within 16 h at room temperature and 72% yield of the desired cycloaddition products (Table 3, entry 6). Finally, by further decreasing its catalytic loading and increasing the reaction concentration, we were able to highlight the outstanding catalytic performance of the $BAr^F{}_4^-$ photosensitizer, which achieved an impressive TON of up to 1040 at a very low loading of 500 ppm (Table 3, entry 7, and the SI).

Table 3. Optimization Using $[Ru(bpy)_3](BAr^F{}_4)_2$ as Catalyst[a]

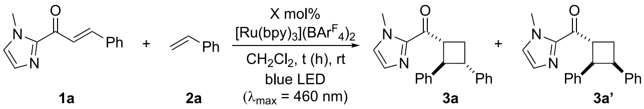

entry	$[Ru(bpy)_3](BAr^F{}_4)_2$ (mol %)	[**1a**] (mol L^{-1})	time (h)	yield (%)[b]	TON[c]
1	2.5	0.05	2	43	17
2	2.5	0.1	2	56	22
3	1	0.1	2	56	54
4	0.5	0.1	2	54	108
5	0.5	0.2	2	70	140
6	0.5	0.2	16	72	144
7	0.05	1.0	16	52	1040

[a] Reaction conditions: **1a** (0.1 mmol), **2a** (1 mmol), $[Ru(bpy)_3](BAr^F{}_4)_2$ (0.05 to 2.5 × 10^{-3} mmol), degassed CH_2Cl_2 (0.25 to 2 mL), and blue LED irradiation (λ_{max} = 460 nm) for 2 to 16 h under Ar. [b] Yield in % of (**3a**+**3a′**) was determined by ^{1}H NMR using 1,3,5-trimethoxybenzene as an internal standard. [c] Turnover number = $n_{(3a+3a')}/n_{Ru}$.

With the optimized conditions in hand, we then investigated the scope of the intermolecular [2 + 2] cycloaddition reaction by first varying the electronic and steric properties of the β-aryl substituent of the α,β-unsaturated 2-acyl *N*-methylimidazole **1** (Table 4). Aryl groups with an electron-donating substituent

Table 4. Scope of *α*,*β*-Unsaturated 2-Acyl *N*-Methylimidazole[a]

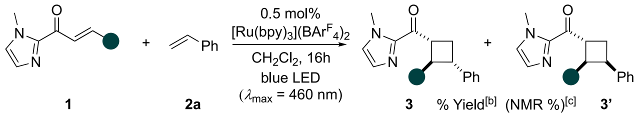

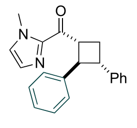 **3a**, 70% (73%) 2.4:1 d.r.[d]	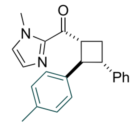 **3b**, 60% (71%) 2.5:1 d.r.[d]	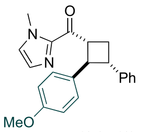 **3c**, 73% (85%) 2.5:1 d.r.[d]	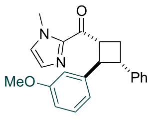 **3d**, 73% (76%) 2.4:1 d.r.[d]
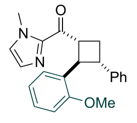 **3e**, 68% (73%) 2.6:1 d.r.[d]	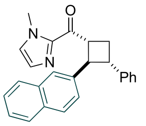 **3f**, 58% (70%) 2:1 d.r.[d]	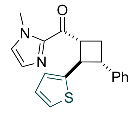 **3g**, 44% (53%) 2.1:1 d.r.[d]	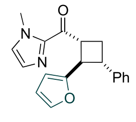 **3h**, 39% (53%) 2.2:1 d.r.[d]
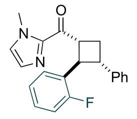 **3i**, 79% (83%) 1.9:1 d.r.[d]	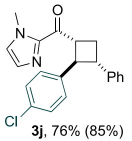 **3j**, 76% (85%) 2.3:1 d.r.[d]	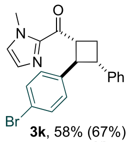 **3k**, 58% (67%) 2:1 d.r.[d]	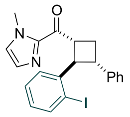 **3l**, nd (10%) 2:1 d.r.[d]
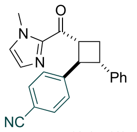 **3m**, 77% (87%) 2.4:1 d.r.[d]	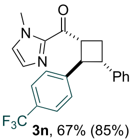 **3n**, 67% (85%) 2.2:1 d.r.[d]	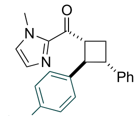 **3o**, 63% (67%) 2.2:1 d.r.[d]	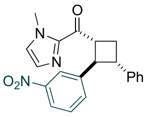 **3p**, 62% (83%) 2.2:1 d.r.[d]

[a] Reaction conditions: **1** (0.2 mmol), **2a** (2 mmol), $[Ru(bpy)_3](BAr^F_4)_2$ (1×10^{-3} mmol), degassed CH_2Cl_2 (1 mL), blue LED irradiation (λ_{max} = 460 nm) for 16 h under Ar. [b] Isolated yield of **3** and **3′**. [c] Yield in % of **3** and **3′** determined by ^1H NMR using 1,3,5-trimethoxybenzene as an internal standard. [d] Diastereomeric ratio (**3**:**3′**) determined by ^1H NMR analysis.

Table 5. Scope of Styrene Partner[a]

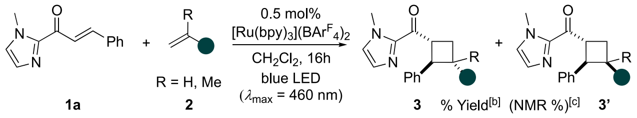

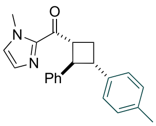 **3q**, 74% (81%) 2.7:1 d.r.[d]	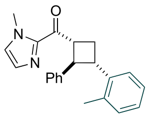 **3r**, 70% (75%) 2.5:1 d.r.[d]	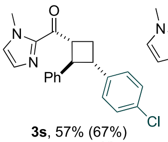 **3s**, 57% (67%) 2.5:1 d.r.[d]	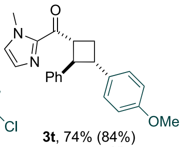 **3t**, 74% (84%) 2.4:1 d.r.[d]
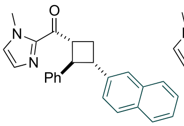 **3u**, 60% (78%) 2.5:1 d.r.[d]	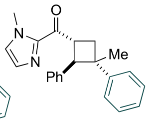 **3v**, 49% (51%) 1.7:1 d.r.[d]	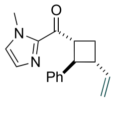 **3w**, 49% (55%) 2.4:1 d.r.[d]	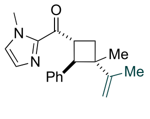 **3x**, 69% (72%) 7.1:1 d.r.[d]

[a] Reaction conditions: **1a** (0.2 mmol), **2** (2 mmol), $[Ru(bpy)_3](BAr^F_4)_2$ (1×10^{-3} mmol), degassed CH_2Cl_2 (1 mL), blue LED irradiation (λ_{max} = 460 nm) for 16 h under Ar. [b] Isolated yield of **3** and **3′**. [c] Yield in % of **3** and **3′** determined by ^1H NMR using 1,3,5-trimethoxybenzene as an internal standard. [d] Diastereomeric ratio (**3**:**3′**) determined by ^1H NMR analysis.

were well tolerated affording the desired products (**3b**−**3e**) in good isolated yields. A slight decrease in yield was nevertheless observed when the steric hindrance increased from a methoxy substituent in the *para*-position (**3c**) to a *meta*-(**3d**) and *ortho*-position (**3e**). Substrate **1f** bearing the bulky 2-naphthyl group also efficiently engaged in the [2 + 2] cycloaddition with styrene to afford the product **3f** in 58% isolated yield. Thienyl and furanyl groups were well tolerated, allowing the formation of products **3g** and **3h** in reasonable yields. With the exception of the *o*-iodophenyl group (**3l**), which induced a very sluggish reaction, substrates bearing an electron-deficient fluoro-, chloro-, bromo-, cyano-, trifluoromethyl, or nitro-aryl group (**3i**−**3p**) were all amenable to efficient cycloaddition catalyzed by the $[Ru(bpy)_3](BAr^F_4)_2$ photocatalyst. We then investigated the scope of the olefin partner, and the results are shown in Table 5. Aryl-substituted electron-rich and electron-poor styrenes, including sterically congested (**2r**), were valuable substrates to afford the desired products (**3q**−**3u**) in good yields. Gratifyingly, the presence of a methyl group at the *α*-position of styrene (**2v**) did not hamper the reactivity. Butadiene and 2,3-dimethylbutadiene are also compatible with the [2 + 2] cycloaddition, allowing the synthesis of cyclobutanes **3w** and **3x** in good yields and with improved 7:1 selectivity in favor of the *trans*−*trans* diastereomer in the latter case. Moreover, the method is not limited to *α*,*β*-unsaturated 2-acyl *N*-methylimidazole **1** since the *N*-methylimidazole moiety can be replaced by other heteroaromatic groups, such as *N*-phenylimidazole (**4a**) or pyridine (**4b**) with no significant impact on the catalytic performance, as demonstrated by the isolation of products (**5a**) and (**5b**) in 72 and 63% yields, respectively (Table 6). Interestingly, energy transfer from the triplet state energy of $[Ru(bpy)_3](BAr^F_4)_2$ to chalcone is also operative in CH_2Cl_2, allowing cycloaddition with styrene to produce the corresponding intermolecular cycloadduct **5c** in a reasonable 44% isolated yield.

Table 6. Scope of *α*,*β*-Unsaturated Ketones[a]

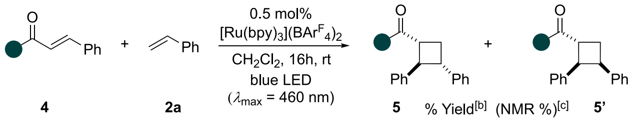

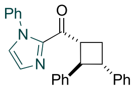 **5a**, 72% (81%) 2.1:1 d.r.[d]	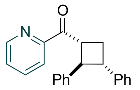 **5b**, 63% (68%) 3.4:1 d.r.[d]	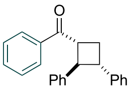 **5c**, 44% (65%) 2.6:1 d.r.[d]

[a] Reaction conditions: **1** (0.2 mmol), **2a** (2 mmol), $[Ru(bpy)_3](BAr^F_4)_2$ (1×10^{-3} mmol), degassed CH_2Cl_2 (1 mL), blue LED irradiation (λ_{max} = 460 nm) for 16 h under Ar. [b] Isolated yield of **5** and **5′**. [c] Yield in % of **5** and **5′** determined by ^1H NMR using 1,3,5-trimethoxybenzene as an internal standard. [d] Diastereomeric ratio (**5**:**5′**) determined by ^1H NMR analysis.

■ CONCLUSIONS

In this work, we reveal counterion effects in triplet−triplet energy transfer processes catalyzed by a cationic transition-metal-based photosensitizer in low-polarity solvent. We observe a strong impact of the counterion identity on the excited-state properties of $[Ru(bpy)_3](X)_2$ photocatalysts and on their capacity to transfer triplet energy to cinnamoyl-type substrates. The limited stabilization by anion−dipole interaction of the $[Ru(bpy)_3]^{2+*}$ excited state in the presence of large $BAr^F{}_4{}^-$ anions in dichloromethane results in a ^{3}MLCT excited state of reduced lifetime but of higher energy, offering an increased driving force for the energy transfer process. In comparison, the efficiency of the energy transfer drops by two orders of magnitude in the presence of small anions like TsO^-. The noncoordinating $BAr^F{}_4{}^-$ anion is also beneficial for the photostability of the cationic photocatalyst by disfavoring the loss of a bpy ligand, which is a predominant decomposition pathway in solvents of low dielectric constant such as dichloromethane in the presence of coordinating/nucleophilic anions. This modulation is due to the fact that $BAr^F{}_4{}^-$ anions favor the population of nondissociative $^3MC_{trans}$ states over dissociative $^3MC_{cis}$ states. Thanks to the excellent photostability and high efficiency in triplet−triplet energy transfer of the $[Ru(bpy)_3](BAr^F{}_4)_2$ photocatalyst in dichloromethane, excellent photocatalytic activities (up to >1000 TON) could be achieved in intermolecular [2 + 2] cycloaddition reactions of broad scope with photocatalyst loading as low as 500 ppm. These results clearly demonstrate that the nature of counterion makes a significant contribution to the potency of cationic photocatalysts, a subtle effect that can also be of prime importance and that has been so far overlooked in the literature regarding photocatalyzed transformations and especially reactions enabled by triplet-triplet energy transfer.

ASSOCIATED CONTENT

Supporting Information

The Supporting Information is available free of charge at https://pubs.acs.org/doi/10.1021/jacsau.4c00384.

General information; photocatalyst synthesis; substrate synthesis; synthesis of racemate [2+2] cycloaddition products; electrochemical data; photophysical experiments; complementary studies; computational studies; X-ray diffraction; and NMR data (PDF)

Cartesian coordinates for all optimized complexes, ground and excited states (ZIP)

AUTHOR INFORMATION

Corresponding Authors

Isabelle M. Dixon − *LCPQ, Université de Toulouse, CNRS, Université Toulouse III - Paul Sabatier, Toulouse F-31062, France;* orcid.org/0000-0001-5551-6715; Email: dixon@irsamc.ups-tlse.fr

Yves Canac − *LCC−CNRS, Université de Toulouse, CNRS, UPS, Toulouse 31077, France;* orcid.org/0000-0002-3747-554X; Email: yves.canac@lcc-toulouse.fr

Michael Smietana − *Institut des Biomolécules Max Mousseron, Université de Montpellier, CNRS, ENSCM, Montpellier 34095, France;* orcid.org/0000-0001-8132-7221; Email: michael.smietana@umontpellier.fr

Olivier Baslé − *LCC−CNRS, Université de Toulouse, CNRS, UPS, Toulouse 31077, France;* orcid.org/0000-0002-4551-473X; Email: olivier.basle@lcc-toulouse.fr

Authors

Juliette Zanzi − *LCC−CNRS, Université de Toulouse, CNRS, UPS, Toulouse 31077, France*

Zachary Pastorel − *Institut des Biomolécules Max Mousseron, Université de Montpellier, CNRS, ENSCM, Montpellier 34095, France*

Carine Duhayon − *LCC−CNRS, Université de Toulouse, CNRS, UPS, Toulouse 31077, France;* orcid.org/0000-0001-7345-8782

Elise Lognon − *ITODYS, Université Paris Cité and CNRS, Paris F-75006, France*

Christophe Coudret − *Université de Toulouse, UPS, Institut de Chimie de Toulouse, FR2599, Toulouse F-31062, France*

Antonio Monari − *ITODYS, Université Paris Cité and CNRS, Paris F-75006, France;* orcid.org/0000-0001-9464-1463

Complete contact information is available at: https://pubs.acs.org/10.1021/jacsau.4c00384

Notes

The authors declare no competing financial interest.

ACKNOWLEDGMENTS

This work was supported by the Centre National de la Recherche Scientifique (CNRS), the Université Toulouse III - Paul Sabatier, the Université de Montpellier, the Région Occitanie Pyrénées-Méditerranée (21012860 "R-SMASH"), and the Agence Nationale de la Recherche (ANR-20-CE07-0021 "SMASH" grant to J.Z., Z.P., Y.C., M.S., and O.B.; ANR-21-CE07-0026 "LYMACATO" grant to Y.C., E. L., and A.M.). The authors thank Charles-Louis Serpentini from Université de Toulouse for excited-state lifetime measurements and INSA Toulouse for luminescence quantum yield measurements. CALMIP is also kindly acknowledged for providing HPC resources (project P18013), as well as the EXplor mesocenter and the national GENCI calculators.

REFERENCES

(1) Candish, L.; Collins, K. D.; Cook, G. C.; Douglas, J. J.; Gómez-Suárez, A.; Jolit, A.; Keess, S. Photocatalysis in the Life Science Industry. *Chem. Rev.* **2022**, *122*, 2907−2980.

(2) Tao, X.; Zhao, Y.; Wang, S.; Li, C.; Li, R. Recent Advances and Perspectives for Solar-Driven Water Splitting using Particulate Photocatalysts. *Chem. Soc. Rev.* **2022**, *51*, 3561−3608.

(3) Banerjee, T.; Podjaski, F.; Kröger, J.; Biswal, B. P.; Lotsch, B. V. Polymer Photocatalysts for Solar-to-Chemical Energy Conversion. *Nat. Rev. Mater.* **2021**, *6*, 168−190.

(4) Zhang, B.; Sun, L. Artificial Photosynthesis: Opportunities and Challenges of Molecular Catalysts. *Chem. Soc. Rev.* **2019**, *48*, 2216−2264.

(5) Luo, J.; Zhang, S.; Sun, M.; Yang, L.; Luo, S.; Crittenden, J. C. A Critical Review on Energy Conversion and Environmental Remediation of Photocatalysts with Remodeling Crystal Lattice, Surface, and Interface. *ACS Nano* **2019**, *13*, 9811−9840.

(6) Angerani, S.; Winssinger, N. Visible Light Photoredox Catalysis Using Ruthenium Complexes in Chemical Biology. *Chem. - Eur. J.* **2019**, *25*, 6661−6672.

(7) Li, X. B.; Tung, C. H.; Wu, L. Z. Semiconducting Quantum Dots for Artificial Photosynthesis. *Nat. Rev. Chem.* **2018**, *2*, 160−173.

(8) Chan, A. Y.; Perry, I. B.; Bissonnette, N. B.; Buksh, B. F.; Edwards, G. A.; Frye, L. I.; Garry, O. L.; Lavagnino, M. N.; Li, B. X.; Liang, Y.; Mao, E.; Millet, A.; Oakley, J. V.; Reed, N. L.; Sakai, H. A.; Seath, C. P.; MacMillan, D. W. C. Metallaphotoredox: The Merger of Photoredox and Transition Metal Catalysis. *Chem. Rev.* **2022**, *122*, 1485−1542.

(9) Sakakibara, Y.; Murakami, K. Switchable Divergent Synthesis Using Photocatalysis. *ACS Catal.* **2022**, *12*, 1857−1878.

(10) Genzink, M. J.; Kidd, J. B.; Swords, W. B.; Yoon, T. P. Chiral Photocatalyst Structures in Asymmetric Photochemical Synthesis. *Chem. Rev.* **2022**, *122*, 1654−1716.

(11) Lunic, D.; Bergamaschi, E.; Teskey, C. J. Using Light to Modify the Selectivity of Transition Metal Catalysed Transformations. *Angew. Chem., Int. Ed.* **2021**, *60*, 20594–20605.

(12) McAtee, R. C.; McClain, E. J.; Stephenson, C. R.J. Illuminating Photoredox Catalysis. *Trends in Chemistry* **2019**, *1*, 111–125.

(13) Marzo, L.; Pagire, S. K.; Reiser, O.; König, B. Visible-Light Photocatalysis: Does It Make a Difference in Organic Synthesis? *Angew. Chem., Int. Ed.* **2018**, *57*, 10034–10072.

(14) Michelin, C.; Hoffmann, N. Photosensitization and Photocatalysis—Perspectives in Organic Synthesis. *ACS Catal.* **2018**, *8*, 12046–12055.

(15) Twilton, J.; Le, C.; Zhang, P.; Shaw, M. H.; Evans, R. W.; MacMillan, D. W. C. The Merger of Transition Metal and Photocatalysis. *Nat. Rev. Chem.* **2017**, *1*, No. 0052.

(16) Romero, N. A.; Nicewicz, D. A. Organic Photoredox Catalysis. *Chem. Rev.* **2016**, *116*, 10075–10166.

(17) Shaw, M. H.; Twilton, J.; MacMillan, D. W. C. Photoredox Catalysis in Organic Chemistry. *J. Org. Chem.* **2016**, *81*, 6898–6926.

(18) Brimioulle, R.; Lenhart, D.; Maturi, M. M.; Bach, T. Enantioselective Catalysis of Photochemical Reactions. *Angew. Chem., Int. Ed.* **2015**, *54*, 3872–3890.

(19) Prier, C. K.; Rankic, D. A.; MacMillan, D. W. C. Visible Light Photoredox Catalysis with Transition Metal Complexes: Applications in Organic Synthesis. *Chem. Rev.* **2013**, *113*, 5322–5363.

(20) Teegardin, K.; Day, J. I.; Chan, J.; Weaver, J. Advances in Photocatalysis: A Microreview of Visible Light Mediated Ruthenium and Iridium Catalyzed Organic Transformations. *Org. Process Res. Dev.* **2016**, *20*, 1156–1163.

(21) Schultz, D. M.; Yoon, T. P. Solar Synthesis: Prospects in Visible Light Photocatalysis. *Science* **2014**, *343*, No. 1239176.

(22) Vlcek, A. A.; Dodsworth, E. S.; Pietro, W. J.; Lever, A. B. P. Excited State Redox Potentials of Ruthenium Diimine Complexes; Correlations with Ground State Redox Potentials and Ligand Parameters. *Inorg. Chem.* **1995**, *34*, 1906–1913.

(23) Henwood, A. F.; Zysman-Colman, E. Lessons Learned in Tuning the Optoelectronic Properties of Phosphorescent Iridium(III) Complexes. *Chem. Commun.* **2017**, *53*, 807–826.

(24) Larsen, C. B.; Wenger, O. S. Photoredox Catalysis with Metal Complexes Made from Earth-Abundant Elements. *Chem. - Eur. J.* **2018**, *24*, 2039–2058.

(25) Hockin, B. M.; Li, C.; Robertson, N.; Zysman-Colman, E. Photoredox Catalysts based on Earth-Abundant Metal Complexes. *Catal. Sci. Technol.* **2019**, *9*, 889–915.

(26) Förster, C.; Heinze, K. Photophysics and Photochemistry with Earth-Abundant Metals – Fundamentals and Concepts. *Chem. Soc. Rev.* **2020**, *49*, 1057–1070.

(27) Wegeberg, C.; Wenger, O. S. Luminescent First-Row Transition Metal Complexes. *JACS Au* **2021**, *1*, 1860–1876.

(28) Herr, P.; Kerzig, C.; Larsen, C. B.; Häussinger, D.; Wenger, O. S. Manganese(I) Complexes with Metal-to-Ligand Charge Transfer Luminescence and Photoreactivity. *Nat. Chem.* **2021**, *13*, 956–962.

(29) de Groot, L. H. M.; Ilic, A.; Schwarz, J.; Wärnmark, K. Iron Photoredox Catalysis–Past, Present, and Future. *J. Am. Chem. Soc.* **2023**, *145*, 9369–9388.

(30) Sinha, N.; Yaltseva, P.; Wenger, O. S. The Nephelauxetic Effect Becomes an Important Design Factor for Photoactive First-Row Transition Metal Complexes. *Angew. Chem., Int. Ed.* **2023**, No. e202303864.

(31) Chan, A. Y.; Ghosh, A.; Yarranton, J. T.; Twilton, J.; Jin, J.; Arias-Rotondo, D. M.; Sakai, H. A.; McCusker, J. K.; MacMillan, D. W. C. Exploiting the Marcus Inverted Region for First-Row Transition Metal–based Photoredox Catalysis. *Science* **2023**, *382*, 191–197.

(32) Troian-Gautier, L.; Beauvilliers, E. E.; Swords, W. B.; Meyer, G. J. Redox Active Ion-Paired Excited States Undergo Dynamic Electron Transfer. *J. Am. Chem. Soc.* **2016**, *138*, 16815–16826.

(33) Li, G.; Swords, W. B.; Meyer, G. J. Bromide Photo-oxidation Sensitized to Visible Light in Consecutive Ion Pairs. *J. Am. Chem. Soc.* **2017**, *139*, 14983–14991.

(34) Morton, C. M.; Zhu, Q.; Ripberger, H. H.; Troian-Gautier, L.; Toa, Z. S. D.; Knowles, R. R.; Alexanian, E. J. C–H Alkylation via Multisite-Proton-Coupled Electron Transfer of an Aliphatic C–H Bond. *J. Am. Chem. Soc.* **2019**, *141*, 13253–13260.

(35) Uraguchi, D.; Kimura, Y.; Ueoka, F.; Ooi, T. Urea as a Redox-Active Directing Group under Asymmetric Photocatalysis of Iridium-Chiral Borate Ion Pairs. *J. Am. Chem. Soc.* **2020**, *142*, 19462–19467.

(36) Xu, J.; Li, Z.; Xu, Y.; Shu, X.; Huo, H. Stereodivergent Synthesis of Both Z- and E-Alkenes by Photoinduced, Ni-Catalyzed Enantioselective C(sp^3)–H Alkenylation. *ACS Catal.* **2021**, *11*, 13567–13574.

(37) Chapman, S. J.; Swords, W. B.; Le, C. M.; Guzei, I. A.; Toste, F. D.; Yoon, T. P. Cooperative Stereoinduction in Asymmetric Photocatalysis. *J. Am. Chem. Soc.* **2022**, *144*, 4206–4213.

(38) Girvin, Z. C.; Cotter, L. F.; Yoon, H.; Chapman, S. J.; Mayer, J. M.; Yoon, T. P.; Miller, S. J. Asymmetric Photochemical [2 + 2]-Cycloaddition of Acyclic Vinylpyridines through Ternary Complex Formation and an Uncontrolled Sensitization Mechanism. *J. Am. Chem. Soc.* **2022**, *144*, 20109–20117.

(39) Farney, E. P.; Chapman, S. J.; Swords, W. B.; Torelli, M. D.; Hamers, R. J.; Yoon, T. P. Discovery and Elucidation of Counteranion Dependence in Photoredox Catalysis. *J. Am. Chem. Soc.* **2019**, *141*, 6385–6391.

(40) Earley, J. D.; Zieleniewska, A.; Ripberger, H. H.; Shin, N. Y.; Lazorski, M. S.; Mast, Z. J.; Sayre, H. J.; McCusker, J. K.; Scholes, G. D.; Knowles, R. R.; Reid, O. G.; Rumbles, G. Ion-Pair Reorganization Regulates Reactivity in Photoredox Catalysts. *Nat. Chem.* **2022**, *14*, 746–753.

(41) Geunes, E. P.; Meinhardt, J. M.; Wu, E. J.; Knowles, R. R. Photocatalytic Anti-Markovnikov Hydroamination of Alkenes with Primary Heteroaryl Amines. *J. Am. Chem. Soc.* **2023**, *145*, 21738–21744.

(42) For an example of counterion effect in iron photoredox catalysis (LMCT emitter), see: Jang, Y. J.; An, H.; Choi, S.; Hong, J.; Lee, S. H.; Ahn, K.-H.; You, Y.; Kang, E. J. Green-Light-Driven Fe(III)$(btz)_3$ Photocatalysis in the Radical Cationic [4 + 2] Cycloaddition Reaction. *Org. Lett.* **2022**, *24*, 4479–4484.

(43) Dutta, S.; Erchinger, J. E.; Strieth-Kalthoff, F.; Kleinmans, R.; Glorius, F. Energy Transfer Photocatalysis: Exciting Modes of Reactivity. *Chem. Soc. Rev.* **2024**, *53*, 1068–1089.

(44) Großkopf, J.; Kratz, T.; Rigotti, T.; Bach, T. Enantioselective Photochemical Reactions Enabled by Triplet Energy Transfer. *Chem. Rev.* **2022**, *122*, 1626–1653.

(45) Zhou, Q.-Q.; Zou, Y.-Q.; Lu, L.-Q.; Xiao, W.-J. Visible-Light-Induced Organic Photochemical Reactions through Energy-Transfer Pathways. *Angew. Chem., Int. Ed.* **2019**, *58*, 1586–1604.

(46) Strieth-Kalthoff, F.; James, M. J.; Teders, M.; Pitzer, L.; Glorius, F. Energy Transfer Catalysis Mediated by Visible Light: Principles, Applications, Directions. *Chem. Soc. Rev.* **2018**, *47*, 7190–7202.

(47) Strieth-Kalthoff, F.; Glorius, F. Triplet Energy Transfer Photocatalysis: Unlocking the Next Level. *Chem.* **2020**, *6*, 1888–1903.

(48) Poplata, S.; Tröster, A.; Zou, Y. Q.; Bach, T. Recent advances in the synthesis of cyclobutanes by olefin [2 + 2] photocycloaddition reactions. *Chem. Rev.* **2016**, *116*, 9748–9815.

(49) Huang, X.; Quinn, T. R.; Harms, K.; Webster, R. D.; Zhang, L.; Wiest, O.; Meggers, E. Direct Visible-Light-Excited Asymmetric Lewis Acid Catalysis of Intermolecular [2 + 2] Photocycloadditions. *J. Am. Chem. Soc.* **2017**, *139*, 9120–9123.

(50) Sherbrook, E. M.; Jung, H.; Cho, D.; Baik, M.-H.; Yoon, T. P. Brønsted Acid Catalysis of Photosensitized Cycloadditions. *Chem. Sci.* **2020**, *11*, 856–861.

(51) Jung, H.; Hong, M.; Marchini, M.; Villa, M.; Steinlandt, P. S.; Huang, X.; Hemming, M.; Meggers, E.; Ceroni, P.; Park, J.; Baik, M.-H. Understanding the Mechanism of Direct Visible-Light-Activated [2 + 2] Cycloadditions Mediated by Rh and Ir Photocatalysts: Combined Computational and Spectroscopic Studies. *Chem. Sci.* **2021**, *12*, 9673–9681.

(52) Sherbrook, E. M.; Genzink, M. J.; Park, B.; Guzei, I. A.; Baik, M. H.; Yoon, T. P. Chiral Brønsted Acid-Controlled Intermolecular Asymmetric [2 + 2] Photocycloadditions. *Nat. Commun.* **2021**, *12*, 5735.

(53) In both solvents, an obvious color change from red to violet is rapidly observed, attesting to the premature decomposition of the photosensitizer under the reaction conditions; see: (a) Jones, R. F.; Cole-Hamilton, D. J. The Substitutional Photochemistry of Tris-(bipyridyl)-Ruthenium(II)Chloride. *Inorg. Chim. Acta* **1981**, *53*, L3−L5. and reference 54

(54) Ward, W. M.; Farnum, B. H.; Siegler, M.; Meyer, G. J. Chloride Ion-Pairing with Ru(II) Polypyridyl Compounds in Dichloromethane. *J. Phys. Chem. A* **2013**, *117*, 8883−8894.

(55) The ion-pairs have little impact on the properties of the ground state of D_3-symmetry, see Durham, B.; Caspar, J. V.; Nagle, J. K.; Meyer, T. J. Photochemistry of $Ru(bpy)_3{}^{2+}$. *J. Am. Chem. Soc.* **1982**, *104*, 4803−4801.

(56) Absorbance and emission spectra of $[Ru(bpy)_3](Cl)_2$ could not be recorded in deoxygenated CH_2Cl_2 due to low solubility and premature decomposition, *vide infra* references 53 and 54.

(57) Kober, E. M.; Sullivan, B. P.; Meyer, T. J. Solvent dependence of metal-to-ligand charge-transfer transitions. Evidence for initial electron localization in MLCT excited states of 2,2'-bipyridine complexes of ruthenium(II) and osmium(II). *Inorg. Chem.* **1984**, *23*, 2098−2104.

(58) Maurer, A. B.; Piechota, E. J.; Meyer, G. J. Excited-State Dipole Moments of Homoleptic $[Ru(bpy')_3]_2{}^{+}$ Complexes Measured by Stark Spectroscopy. *J. Phys. Chem. A* **2019**, *123*, 8745−8754.

(59) Alary, F.; Heully, J.-L.; Bijeire, L.; Vicendo, P. Is the ^{3}MLCT the Only Photoreactive State of Polypyridyl Complexes? *Inorg. Chem.* **2007**, *46*, 3154−3165.

(60) Vining, W. J.; Caspar, J. V.; Meyer, T. J. The Influence of Environmental Effects on Excited-State Lifetimes. The effect of Ion Pairing on Metal-to-Ligand Charge Transfer Excited States. *J. Phys. Chem.* **1985**, *89*, 1095−1099.

(61) Triplet excited state energies (E_T) were estimated from the emission maxima recorded at room temperature, see: Caspar, J. V.; Meyer, T. J. Photochemistry of $Ru(bpy)_3{}^{2+}$. Solvent Effects. *J. Am. Chem. Soc.* **1983**, *105*, 5583−5590.

(62) Buzzetti, L.; Crisenza, G. E. M.; Melchiorre, P. Mechanistic Studies in Photocatalysis. *Angew. Chem., Int. Ed.* **2019**, *58*, 3730−3747.

(63) Schmid, L.; Kerzig, C.; Prescimone, A.; Wenger, O. S. Photostable Ruthenium(II) Isocyanoborato Luminophores and Their Use in Energy Transfer and Photoredox Catalysis. *JACS Au.* **2021**, *1*, 819−832.

(64) Soupart, A.; Dixon, I. M.; Alary, F.; Heully, J. L. DFT Rationalization of the Room-Temperature Luminescence Properties of $Ru(bpy)_3{}^{2+}$ and $Ru(tpy)_2{}^{2+}$: ^{3}MLCT−^{3}MC Minimum Energy Path from NEB Calculations and Emission Spectra from VRES Calculations. *Theor. Chem. Acc.* **2018**, *137*, 37.

(65) Strauss, S. H. The Search for Larger and More Weakly Coordinating Anions. *Chem. Rev.* **1993**, *93*, 927−942.

(66) For a recent study highlighting the critical role of cage escape in photoredox reactions, see: Wang, C.; Li, H.; Bürgin, T. H.; Wenger, O. Cage escape governs photoredox reaction rates and quantum yields. *Nat. Chem.* **2024**, *16*, 1151−1159.

(67) Goodwin, M. J.; Dickenson, J. C.; Ripak, A.; Deetz, A. M.; McCarthy, J. S.; Meyer, G. J.; Troian-Gautier, L. Factors that Impact Photochemical Cage Escape Yields. *Chem. Rev.* **2024**, *124*, 7379−7464.

(68) Soupart, A.; Alary, F.; Heully, J. L.; Elliott, P. I. P.; Dixon, I. M. Exploration of Uncharted ^{3}PES Territory for $[Ru(bpy)_3]^{2+}$: A New ^{3}MC Minimum Prone to Ligand Loss Photochemistry. *Inorg. Chem.* **2018**, *57*, 3192−3196.

(69) Soupart, A.; Alary, F.; Heully, J.-L.; Dixon, I. M. On the Possible Coordination on a ^{3}MC State Itself? Mechanistic Investigation Using DFT-Based Methods. *Inorganics* **2020**, *8*, 15.

(70) Soupart, A.; Alary, F.; Heully, J.-L.; Elliott, P. I. P.; Dixon, I. M. Theoretical Study of the Full Photosolvolysis Mechanism of $[Ru(bpy)_3]^{2+}$: Providing a General Mechanistic Roadmap for the Photochemistry of $[Ru(N^\wedge N)_3]^{2+}$-Type Complexes toward Both Cis and Trans Photoproducts. *Inorg. Chem.* **2020**, *59*, 14679−14695.

(71) Eastham, K.; Scattergood, P. A.; Chu, D.; Boota, R. Z.; Soupart, A.; Alary, F.; Dixon, I. M.; Rice, C. R.; Hardman, S. J. O.; Elliott, P. I. P. Not All ^{3}MC States Are the Same: The Role of $^3MC_{cis}$ States in the Photochemical N^N Ligand Release from $[Ru(bpy)_2(N^\wedge N)]^{2+}$ Complexes. *Inorg. Chem.* **2022**, *61*, 19907−19924.